Journal of Alloys and Compounds 676 (2016) 499–504

Contents lists available at ScienceDirect

Journal of Alloys and Compounds

journal homepage: http://www.elsevier.com/locate/jalcom

Spark plasma texturing (SPT) of *p-type* $[Ca_2CoO_3]_{0.62}[CoO_2]$ thermoelectric oxide

J.G. Noudem [a, b, *], R. Retoux [a], S. Lanfredi [c]

[a] LUSAC EA 4253, UNICAEN, Rue Aragon, 50130 Cherbourg, France
[b] CRISMAT UMR 6508-CNRS, UNICAEN, 6Bd Maréchal Juin, 14050 Caen Cedex 4, France
[c] Fac de Ciências e Tecnologia–FCT, Univ Estadual Paulista – UNESP, P.O Box 467, Presidente Prudente, SP, 19060-900, Brazil

ARTICLE INFO

Article history:
Received 16 July 2015
Received in revised form
7 March 2016
Accepted 11 March 2016
Available online 16 March 2016

Keywords:
P-type thermoelectric oxide material
Calcium cobaltate
Spark plasma sintering-Texturation
Grain growth

ABSTRACT

Hole-doped $[Ca_2CoO_3]_{0.62}[CoO_2]$ (Co349) thermoelectric materials were densified and textured by spark plasma sintering (SPS) process. Thin pre-sintered Co349 lamellar samples were used to process textured monoliths. The textured thin monoliths were further used in obtaining samples with increased thickness for anisotropic property studies by hot-stacking as multiple layers. Infrared measurements were used to investigate the presence of carbon diffused from the SPS tool into the bulk of the sample. The phase compositions, grain texture, as well as microstructure of the samples were analyzed by X-ray diffraction and SEM studies. The high temperature thermoelectric transport properties of the bulk samples and the correlation between the grain orientations, structural and anisotropy of thermoelectric properties were discussed in detail. The textured sample processed by SPT shows the power factor value of 450 $\mu W\ m^{-1}\ K^{-2}$ at 600 °C which is 30% higher than the corresponding value for SPS one and eight times larger than samples conventionally sintered.

1. Introduction

Since the discovery of thermoelectric (TE) oxide [1], the misfit layered $[Ca_2CoO_3]_q[CoO_2]$ compound is one of the most studied *p-type* system [2–11] for high temperature applications. The compound was most reported with $Ca_3Co_4O_9$ formula, but the appropriate misfit layered structure expression $[Ca_2CoO_3]_q[CoO_2]$ was revealed in 2000 [2,3]. The value of q = 0.62 was determined by Y. Miyazaki et al. [5] from a precise structure analysis based on neutron and X-ray powder diffraction data and superspace group approach.

Besides its TE performance, the layered cobaltite oxide is also known for its high oxidation resistance, excellent chemical and high temperature stabilities in air and containing no toxic elements. Several efforts have been reported in further enhancing the thermoelectric properties of calcium cobaltate oxide $[Ca_2CoO_3]_{0.62}[CoO_2]$, such as: (i) Partial element substitution at Ca, and/or Co sites in optimizing the carrier concentration with various elements such as alkali metals, alkaline earth metals, rare earth or transition metals [8,12–16]. (ii) Processing of the grain-oriented bulk materials is another mostly investigated method for improving the thermoelectric properties. The magnetic alignment method [17], reactive template grain growth technique [18], hot-pressing, HP [7,19,20], Spark Plasma Sintering, SPS and/or Texturing, SPT [10,11,21,22] are also reported in obtaining dense and texture layered cobaltite thermoelectric materials. These efforts are also evidenced by the numerous recent publications [23–26]. Few authors reported that, the $[Ca_2CoO_3]_{0.62}[CoO_2]$ single crystal had a dimensionless figure of merit, ZT = 0.83 at 973 K [27], however the crystal sizes are still small for device applications. An alternative way to single crystals is to use the grain aligned polycrystalline bulk materials.

We have recently reported [22] that SPT is very effective technique for processing of dense and textured $[Ca_2CoO_3]_{0.62}[CoO_2]$ pellets with a significant (*a*, *b*) planes grain growth, which reduces significantly their electrical resistivity and consequently, improves the power factor.

Nevertheless, the obtained textured pellets are still thin (with a mean thickness of about 0.7 mm) to design TE 'legs' for device application, which typically require larger dimensions [28–30]. To overcome this issue, we have processed thick samples by hot-stacking the textured $[Ca_2CoO_3]_{0.62}[CoO_2]$ pellets by using SPS

* Corresponding author. CRISMAT UMR 6508-CNRS, UNICAEN, 6Bd Maréchal Juin, 14050 Caen Cedex 4, France. Fax: +33 231451309.
E-mail address: jacques.noudem@ensicaen.fr (J.G. Noudem).

http://dx.doi.org/10.1016/j.jallcom.2016.03.063
0925-8388/

technique and further characterized their TE properties. Compare to our previous report [22], the thick samples were obtained in order to investigate: (i) the thermoelectric anisotropy properties and (ii) to design the thermoelectric legs for modules. Infrared measurements were firstly used to investigate the graphite diffusion into the bulk sample. X-ray diffraction has been used to investigate the phase compositions, grain alignment along the parallel and perpendicular directions w.r.t applied pressure and microstructure analyses have been used to confirm the same. The high temperature thermoelectric transport properties of the bulk samples and the correlation between the grain orientations, structural and anisotropy in thermoelectric properties are discussed in detail.

2. Experimental procedures

The $Ca_3Co_4O_9$ powder was prepared by conventional solid-state reaction as described in detail elsewhere [6,7]. Briefly, pure Co_3O_4 oxide and $CaCO_3$ carbonate were mixed, calcined (900 °C, 12 h) and pressed uniaxially (30 MPa) into pellets. The reference samples were heated at 920 °C for 24 h in air for conventional sintering (CS). Other samples were further heat treated using regular Spark Plasma Sintering-SPS and edge free deformation namely spark plasma texturing-SPT processing as described elsewhere [10,11,22]. Several single pieces of SPT pellets (Fig. 1a) were well polished, stacked (Fig. 1b) without using any soldering agent and treated at 900 °C for 10 min under a moderate force of 5 kN. The as hot-stacked sample is shown in Fig. 1c having a thickness of ~10 mm. According to the processing conditions, the samples were named: SPS-ab, SPS-c, SPT-ab and SPT-c where (ab) and (c) means in and out-of-the planes, respectively. Before structural and thermoelectric investigations, infrared studies have been undertaken for analyzing the carbon diffusion during the SPS process into the samples. The samples were characterized; basically, the chemical bonds were analyzed by infrared spectroscopy (FTIR). Measurements were carried out with an instrument resolution of 1 cm^{-1} in the range of 4000–500 cm^{-1} for 100 scans using a Fourier transform spectrometer, Model Digilab Excalibur (FTS 3100 HE series). To investigate the carbon contamination, the transmittance was performed on different samples: (i) the as processed, SPS1 sample where the graphite foil "Papyex" was just removed without any polishing and additional annealing. (ii) The SPS2 was annealed at 800 °C, 2 h in air. (iii) Finally, SPS3 was polished after annealing. These three samples were compared with the reference, CS sample. The transmittance curves (Fig. 2) show the bands at 2339 and 2361 cm^{-1} corresponding to the normal vibrational modes of CO_2. The transmittance peak is higher for the SPS1 sample than SPS2. The transmittance of the SPS3 sample is close to the CS one. This preliminary study demonstrates that, after initial Spark Plasma Sintering process, the as-processed samples need to be carefully prepared before the basic characterizations. The chemical specimen composition after processing and the texture of the samples were investigated using XRD measurements on Philips apparatus with CuK_α radiation. Scanning electron microscopy-SEM (Supra 55, Oberkochen, Germany) was employed to analyze the microstructures.

In addition, the transmission electron microscopy-TEM was further used to investigate the finer microstructural features. The Energy Dispersive Analysis and High Resolution Electron Microscopy observations were performed at room temperature on 200 kV JEOL 2010 FEG STEM electron microscopes (tilt ± 42°) equipped with an EDS (Energy Dispersive Spectrometer, Si/Li detector) EDAX and fitted with double tilt sample holder. Cross sections of bulk samples for TEM observations were prepared by ion milling (Ar gas) at low voltage to prevent heat damages during the preparation using a JEOL Ion Slicer.

The high temperature measurements (sample size: 2 mm × 2 mm × 10 mm) of electrical resistivity, ρ, and Seebeck coefficient, S, were simultaneously monitored by means of a ZEM-3 apparatus (ULVAC-RIKO, Inc, Japan) and the four-probe method. The potential voltage measurement or the applied current was parallel and perpendicular to the applied pressure during processing. In the other word, the current applied or the measured voltage were in-plane or out of the planes of the bar samples cutting from hot-stacked SPT disc with respect to the direction of the pressure applied during processing.

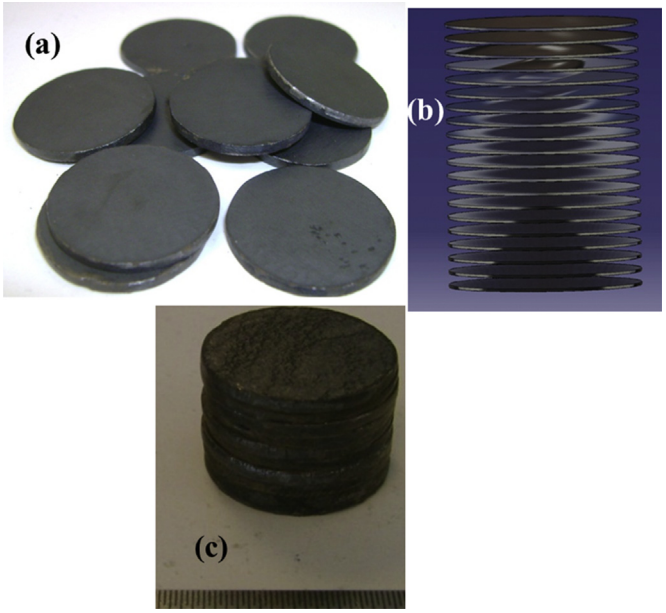

Fig. 1. (a) As-processed discs. (b) Schematic diagram of the stacking. (c) Thick $Ca_3Co_4O_9$ *p-type* thermoelectric after SPS hot-stacking.

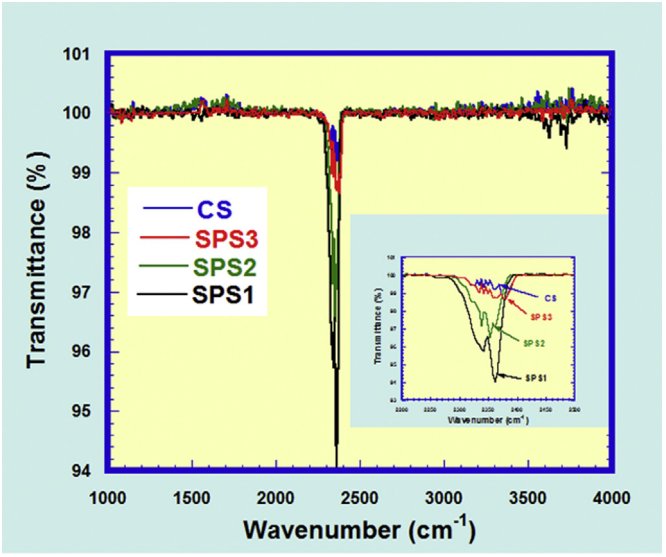

Fig. 2. Transmittance curves of the conventional sintered (CS), as-processed (SPS1), annealed (SPS2) and polished (SPS3) samples.

3. Results and discussion

3.1. XRD

Fig. 3 shows the XRD patterns of CS, SPS-ab, SPS-c, SPT-ab and SPT-c samples for the surface perpendicular and parallel to the applied pressure direction during processing. The patterns show the single-phase nature of the powders with no secondary or impurity phases. All the peaks were indexed as on XRD patterns of CS sample. This indexation including satellite reflections originated from the misfit-layered structure was made according to some works [8,9] reported elsewhere. The faces perpendicular to the applied pressure (SPS-c and SPT-c samples) reveal strong (00ℓ) reflections. The SPT-c sample exhibits more intense (00ℓ) peaks than the SPS-c sample. On the other hand, some diffractions from other crystal planes as (hkl) still exists in the case of SPS-c sample. These features could be correlated to the microstructures, where the SPT-c shows the well aligned lamellar platelets in contrast to SPS-c micrograph. In our previous work [22] we report that, the CS sample exhibits no crystallographic texture. The results from the quantitative texture analysis of the samples processed by SPS reveal an increase of the texture strength. Indeed, the maximum of {001} pole figure is culminated at 7.63 m.r.d at the center of {001} for the SPT sample. This indicates that the grains tend to be transformed into larger platelets and the <001> directions to be aligned parallel to the stress axis, notably for the sample sintered at high temperature, in agreement with the SEM observations.

3.2. Microstructure and densities

The SEM pictures of the faces broken parallel and perpendicular to the applied processing pressure axis are shown in Fig. 4. The images of SPS and SPT samples taken at the same magnification show a homogeneous and dense microstructures. From sample mass and volume determinations, the relative density of all samples is about 98% of the theoretical value [2]. We can compare this density with the value of 60% obtained for the sample processed by conventional sintering. In this case, the grains are randomly distributed and loosely assembled (Fig. 4a). The microstructures of the SPS sample (Fig. 4 b and c) seem similar when the applied pressure axis is parallel and perpendicular. Basically, the platelets exhibit no preferential direction, except at some small zones where we can observe the grain alignment. The comparison with the SPT sample shows, (i) the high degree of orientation of large platelets compactly stacked up along the applied pressure axis (Fig. 4d). (ii) Fig. 4e also, shows the large grains where the average c-axis (as confirmed by XRD, Fig. 3, SPT-c) is parallel to the applied pressure. The comparison of Fig. 4b and d demonstrates the detrimental influence of the mold wall on the morphology of these lamellar materials. In fact, the microstructure of the SPT sample is similar to the one usually obtained with the hot-pressing process [6,7,19]. We can conclude that, the Edge-free Spark Plasma Sintering or Spark Plasma Texturing (SPT) is favorable for the grain growth and allows inducing good alignment among the grains, required for improved transport properties. The TEM study clearly confirms the SEM analyses. EDS measurements performed on numerous grains are in good agreement with the nominal $Ca_3Co_4O_9$ chemical composition of the samples and Fig. 4f presents the typical aspect of the prepared cross sections. An enlargement region is shown as insert in Fig. 4f. These TEM observations at micro and nano scales confirm the high density of the specimens. The stacking of the grains do not show any defects and no free spaces are evidenced. The high resolution image presented in inset attests the good crystallinity of the samples. At lower resolution, the observed grains present two type of contrasts, some with very regular attesting of this good and regular crystallinity of the samples and some with quite perturbed contrasts which probably could be the result of the presence of strains in the particular grains. Further investigations using High Resolution Electron Microscopy are in progress for in-depth understanding of these phenomena.

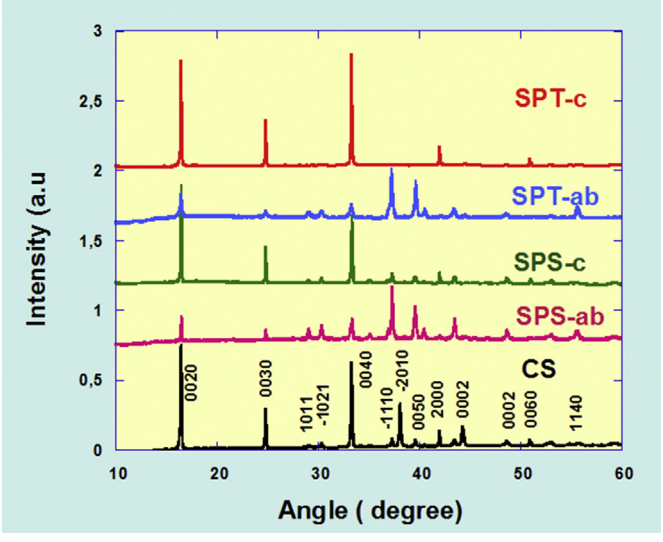

Fig. 3. XRD diffraction curves obtained, from the face perpendicular (c-axis) and parallel (ab-planes) to the applied pressure during Spark Plasma Sintering (SPS) and Spark Plasma Texturing (SPT).

3.3. Thermoelectric properties

The thermoelectric measurements are depicted in Fig. 5. Fig. 5a shows the temperature dependence of the electrical resistivity, ρ. The measurements were performed on the conventional sintering (CS), Spark Plasma Sintering, Spark Plasma Texturing and labeled as ρ_{CS}, ρ_{SPS} and ρ_{SPT}, respectively. For the SPS and SPT samples, the electrical resistivities have been measured in parallel and perpendicular directions to the applied pressure during sample processing. As expected, the electrical resistivity of the samples processed by Spark Plasma Sintering and Texturing exhibit an anisotropy (inset Fig. 5a). The resistivity values with respect to parallel direction of the applied pressure (ρ_c) are greater than the perpendicular direction (ρ_{ab}). It may be noticed that, the anisotropy of the SPT sample is higher than SPS one. This can be correlated to the microstructure shown in Fig. 4 where the SPT exhibits strong alignment of platelets. The anisotropic resistivity behavior versus temperature is presents by inset of Fig. 5a. The SPT curve is above the SPS one. The anisotropy factor decrease slightly with the temperature but remain almost constant at 350 °C with further increasing temperature. The anisotropy values at 150 °C are estimated to be $\rho_{SPT-c}/\rho_{SPT-ab} = 7$ and $\rho_{SPS-c}/\rho_{SPS-ab} = 2.3$ for SPT and SPS samples respectively. This anisotropy value is higher up to 20 above room temperature for the single crystal reported by A–C Masset et al. The authors show that the in-plane resistivity curve, ρ_{ab} (T) measured on single crystal is quite similar to the ρ(T) performed on ceramic sample. The resistivity curve of the CS sample is well above the SPS and SPT ones. It is clear that the SPT and SPS lead to decrease in resistivity values due to the enhancement to the sample density and alignment of the grains. In the other word the grain boundaries density. At 200 °C, $\rho_{SPT-ab} = 9$ and $\rho_{SPS-ab} = 11$ mΩ cm as compared to CS sample ($\rho_{CS} = 35$ mΩ cm). The higher values of the electrical resistivity are due to the low density and random orientation of the grains in the CS sample. On

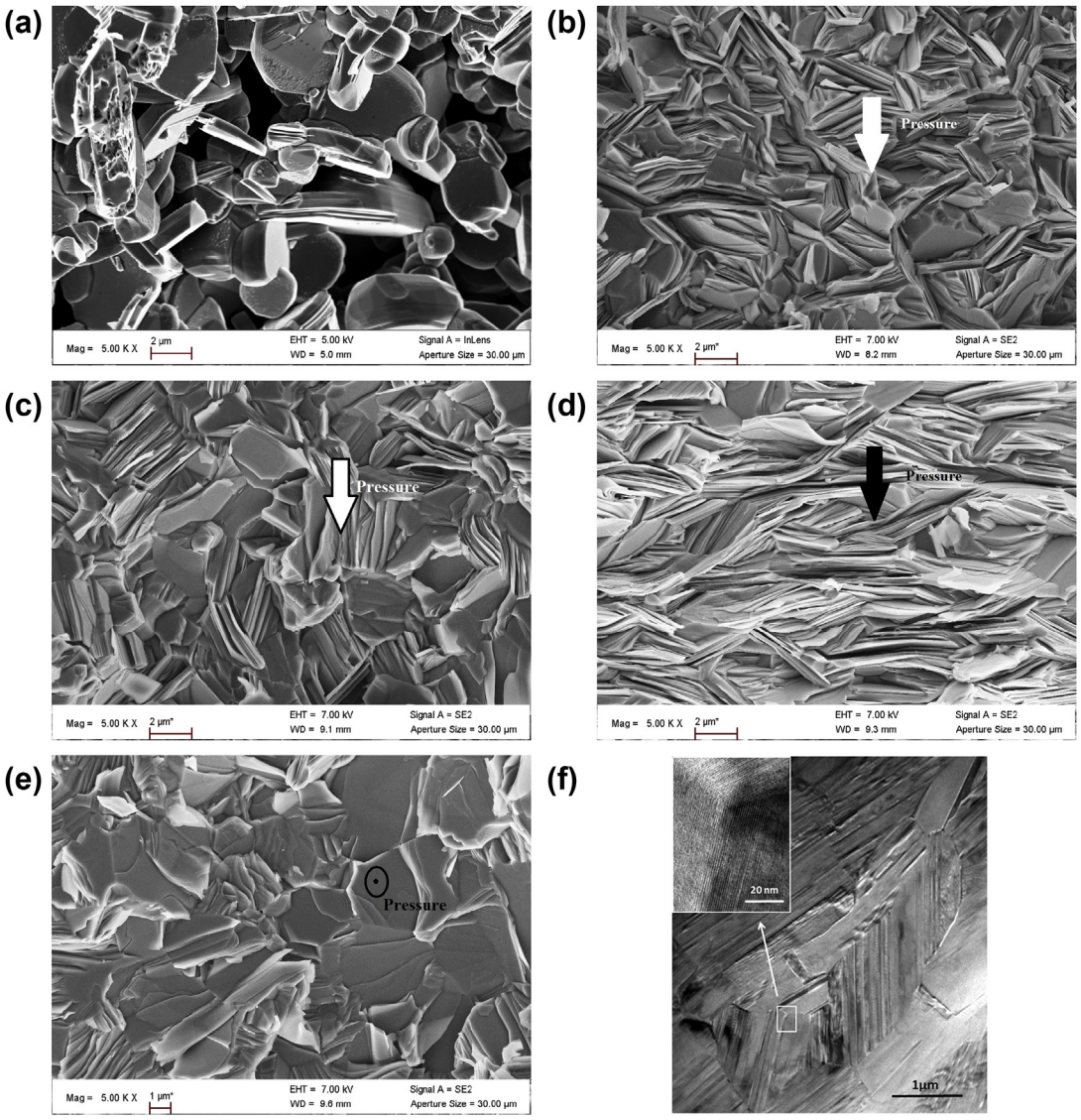

Fig. 4. SEM micrographs of (a) the Conventional Sintered (CS) $Ca_3Co_4O_9$ *p-type* thermoelectrics. (b) Spark Plasma Sintering-SPS, face parallel to the applied pressure (c) SPS, face perpendicular to the applied pressure. (d) Spark Plasma Texturing-SPT sample, face parallel to the applied pressure and (e) SPT, face perpendicular to the applied pressure. (f) TEM micrograph of the SPT sample showing the good connectivity between grains and the crystallinity (insert) of the sample.

the other hand, all curves show a transition around 350 °C. This transition is attributed by some authors [2,31] due to the magnetic transition or structural transition and has been discussed elsewhere [22]. At low temperatures, the resistivity of the conventionally sintered sample, ρ_{CS}, as compared to the Spark Plasma Texturing, lies between the, ρ_{SPT-c}, ρ_{SPT-ab} curves, closer to the, ρ_{SPT-c} curve than, ρ_{SPT-ab} curve one in the ratio of 1/3 before magnetic transition, in agreement with the statistical random distribution of the grains. This can be also correlated to the SEM image showed in Fig. 4a, d, and e. On the other hand, the resistivity of the conventional sintering sample, ρ_{CS} is lower than ρ_{SPT-c}, because in the case of the SPT-c, the current should cross layer by layer with respect to the conventional sintering sample where there are two components of the current: in-planes and out-of- the plane contributions. It seems also that grain boundaries density is higher for the SPT-c sample than the conventional sintering one. This can be clearly observed on Fig. 4a and e respectively.

The temperature dependence of the thermoelectric power or Seebeck coefficient, S, shows *p-type* thermoelectric material within the explored temperature range. This *p-type* behavior indicates that the hole carriers dominate the transport properties. On the other hand, the thermoelectric power is insensitive to grain orientation. The values measured on the both directions are quite close. Similar results were reported by some authors [11]. An explanation of the anisotropic behavior seems to related to the tensorial expression [7] of the Seebeck coefficient showing that the in-planes (ab-planes) component is more pronounced than out-of-the plane (c-axis).

The evolution of the power factor ($PF = S^2/\rho$), deduced from resistivity, ρ, and Seebeck coefficient, S, measurements are shown in the same figure. The power factor of SPS and SPT samples reached at 600 °C, 350 and 450 $\mu W/m/K^2$ respectively. The highest value of 450 $\mu W/m/K^2$ at 600 °C clearly shows the advantage of SPT process with respect to the Spark Plasma Sintering or other methods performed at similar temperatures[5, 21]. This power factor value of SPT sample is almost 30% higher than the corresponding value for SPS, and eight times larger than samples conventionally sintered [22]. From in-plane values at 300 K of single crystal

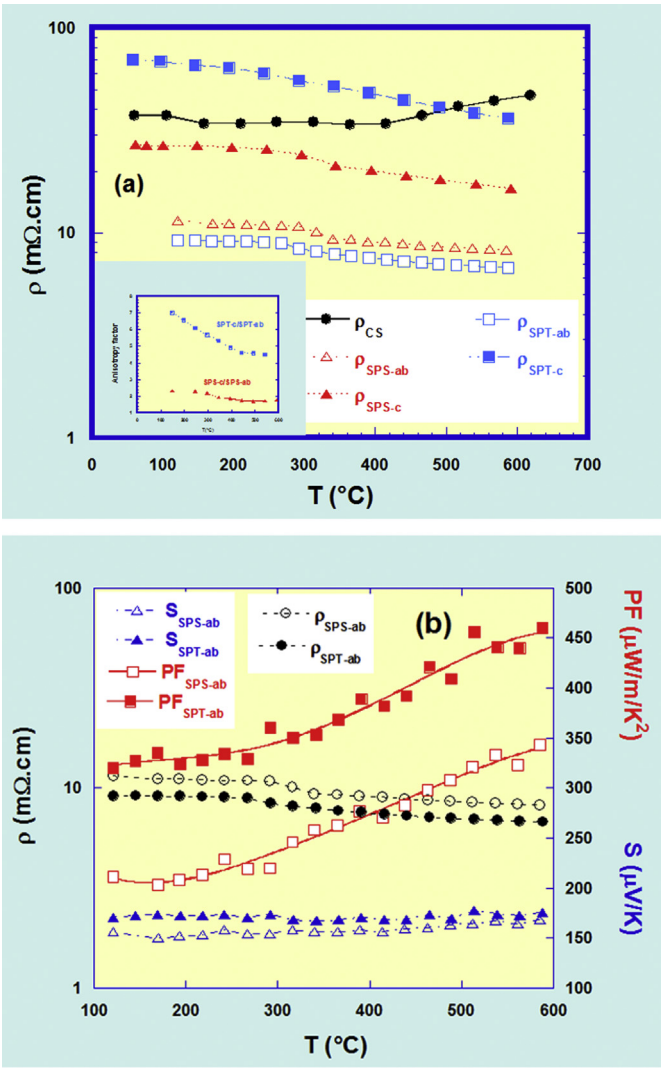

Fig. 5. (a) Temperature dependence of the electrical resistivity on the conventional sintering (CS) sample, in and out-planes samples processed by SPS and SPT respectively (The inset showing the anisotropy factor of the both samples). (b) Temperature dependence of electrical resistivity (round symbols), Seebeck coefficient (triangle symbol) and Power factor (square symbols) curves for samples processed by SPS (open symbols) and SPT (plain symbols) respectively.

reported elsewhere we can calculate the power factor of ~160 μW/m/K^2. This value is comparable to the value deduce at room temperature from our in-plane SPT sample. An open question is the difference about the in-plane power factor of hot-staked SPT sample compare to mono layer of SPT. In our previous work [22], the power factor was performed on the single layer sample compare to this work where several single layers were hot-staked. The power factor is defined as S^2/ρ (S: Seebeck coefficient, ρ: resistivity). But, the resistivity, ρ, is sensitive to the grain boundary. In the case of multiple layers sample, there are more grain boundaries and this could affected the power factor.

4. Conclusions

The Spark Plasma Texturing (SPT) method is highly effective in improving the thermoelectric properties of $[Ca_2CoO_3]_{0.62}[CoO_2]$ oxide ceramics. We successfully processed dense and textured bulk $[Ca_2CoO_3]_{0.62}[CoO_2]$ ceramic materials by combining the SPT and hot-stacking process. The microstructure studies showed a good connectivity and alignment between grains. The transport properties indicted that the electrical resistivity of the SPT sample is lower than the conventional SPS samples, leading to an anisotropic resistivity up to 2.7 times between the both SPT and SPS processes. The power factor of the SPT sample reached 450 μW/m/K^2 at 600 °C, which is one of the highest values for $[Ca_2CoO_3]_{0.62}[CoO_2]$ ceramic reported for the measured temperature. It has been demonstrated that bulk textured thermoelectric 'legs', can be obtained by stacking multilayer $[Ca_2CoO_3]_{0.62}[CoO_2]$ samples without using any soldering agent. The SPT could be a new way to prepare the next generation of any lamellar structure of thermoelectric materials. The outlook of this work will be to perform the thermal conductivity measurements in order to estimate the figure of merit of SPT samples.

Acknowledgments

The authors thank J. Lecourt and F-X. Lefevre for technical support, M. Strebel and X. Larose for sample preparation for TEM studies, Msc. Manoela Romero Besse for infrared spectroscopy measurements assistance and Dr. E. S. Reddy for reading this paper.

References

[1] I. Terasaki, Y. Sasago, K. Uchinokura, Large thermoelectric power in $NaCo_2O_4$ single crystals, Phys. Rev. B 56 (1997) R12685–R12687.
[2] A.C. Masset, C. Michel, A. Maignan, M. Hervieu, O. Toulemonde, F. Studer, B. Raveau, J. Hejtmanek, Misfit-layered cobaltite with an anisotropic giant magnetoresistance: $Ca_3Co_4O_9$, Phys. Rev. B 62 (2000) 166–175.
[3] Yuzuru Miyazaki, Kazutaka Kudo, Megumi Akoshima, Yasuhiro Ono, Yoji Koike, Tsuyoshi Kajitani, Low-temperature thermoelectric properties of the composite crystal [Ca $_2$CoO $_{3.34}$] $_{0.614}$[CoO $_2$], Jpn. J. Appl. Phys. 39 (2000) 531–533.
[4] A. Maignan, S. Hebert, L. Pi, D. Pelloquin, C. Martin, C. Michel, M. Hervieu, B. Raveau, Perovskite manganites and layered cobaltites: potential materials for thermoelectric applications, Cryst. Eng. 5 (2002) 365–382.
[5] Y. Miyazaki, M. Onoda, T. Oku, M. Kikuchi, Y. Ishii, Y. Ono, Y. Morii, T. Kajitani, Modulated structure of the thermoelectric compound [Ca2CoO3]0.62CoO2, J. Phys. Soc. Jpn. 71 (2002) 491–497.
[6] M. Prevel, S. Lemonnier, Y. Klein, S. Hébert, D. Chateigner, B. Ouladdiaf, J.G. Noudem, Textured $Ca_3Co_4O_9$ thermoelectric oxides by thermoforging process, J. Appl. Phys. 98 (2005) 093706–093709.
[7] D. Kenfaui, B. Lenoir, D. Chateigner, B. Ouladdiaf, M. Gomina, J.G. Noudem, Development of multilayer textured $Ca_3Co_4O_9$ materials for thermoelectric generators: Influence of the anisotropy on the transport properties, J. Eur. Ceram. Soc. 32 (2012) 2405–2414.
[8] Y. Miyazaki, T. Miura, M. Onoda, M. Uchida, Y. Ishii, Y. Ono, Y. Morii, T. Kajitani, Modulated structure of misfit-layered cobalt oxide $[Ca_2(Co_{0.65}Cu_{0.35})_2O_4]_{0.63}$-$CoO_2$, Jpn. J. Appl. Phys. 42 (2003) 7467–7473.
[9] Y. Oide, Y. Miyazaki, Y. Ono, X.Y. Huang, T. Kajitani, Thermogravimetric study and high-temperature thermoelectric properties of $[Ca_2(Co_{1-x}A_x)O_3]_{0.62}CoO_2$, in: Proc. Int. Conf. Thermoelectr. (ICT2006) IEEE, 2006, pp. 402–405.
[10] D. Kenfaui, G. Bonnefont, D. Chateigner, G. Fantozzi, M. Gomina, J.G. Noudem, $Ca_3Co_4O_9$ ceramics consolidated by SPS process: optimization of mechanical and thermoelectric properties, Mat. Res. Bull. 45 (2010) 1240–1249.
[11] Y. Zhang, J. Zhang, Q. Lu, Synthesis of highly textured $Ca_3Co_4O_9$ ceramics by spark plasma sintering, Ceram. Int. 33 (2007) 1305–1308.
[12] P.-H. Xiang, Y. Kinemuchi, H. Kaga, K. Watari, Fabrication and thermoelectric properties of $Ca_3Co_4O_9$/Ag composites, J. Alloys Compd. 454 (2008) 364–369.
[13] D. Wang, L. Chen, Q. Wang, J. Li, High-temperature thermoelectric properties of $Ca_3Co_4O_{9+\delta}$ with Eu substitution Solid, State. Comm. 129 (2004) 615–618.
[14] D. Wang, L. Chen, Q. Wang, J. Li, Fabrication and thermoelectric properties of $Ca_{3-x}Dy_xCo_4O_{9+\delta}$ system, J. Alloys Compd. 376 (2004) 58–61.
[15] Y. Lu, Y. song, J. Feng, F.P. Wang, Effects of Ag addition on high temperature thermoelectric properties of $(Ca_{0.9}Gd_{0.1})_3Co_4O_9$ ceramics, Mater Sci. Forum 650 (2010) 132–136.
[16] Y. Song, Q. Sun, L.R. Zhao, F.P. Wang, Synthesis and thermoelectric power factor of $(Ca_{0.95}Bi_{0.05})_3Co_4O_9$/Ag composites, Mater. Chem. Phys. 113 (2009) 645–679.
[17] S. Horii, I. Matsubara, M. Sano, K. Fujie, M. Suzuki, R. Funahashi, M. Shikano, W. Shin, N. Murayama, J.-I. Shimoyama, K. Kishio, Thermoelectric performance of magnetically c-axis aligned Ca-based cobaltites, Jpn. J. Appl. Phys. 42 (2003) 7018–7022.
[18] H. Itahara, C. Xia, J. Sugiyama, T. Tani, Fabrication of textured thermoelectric layered cobaltites with various rock salt-type layers by using β-$Co(OH)_2$ platelets as reactive templates, J. Mater. Chem. 14 (2004) 61–66.
[19] D. Kenfaui, D. Chateigner, M. Gomina, J.G. Noudem, Texture, mechanical and

thermoelectric properties of Ca3Co4O9 ceramics, J. Alloys Compd. 490 (2010) 472–479.
[20] D. Kenfaui, D. Chateigner, M. Gomina, J.G. Noudem, Anisotropy of the mechanical and thermoelectric properties of hot-pressed single-layer and multilayer thick $Ca_3Co_4O_9$ ceramics, Int. J. Appl. Ceram. Technol. 8 (2011) 214–226.
[21] Y. Liu, Y. Lin, Z. Shi, C.-W. Nan, Z. Shen, Preparation of Ca3Co4O9 and improvement of its thermoelectric properties by spark plasma sintering, J. Am. Ceram. Soc. 88 (2005) 1337–1340.
[22] J.G. Noudem, D. Kenfaui, D. Chateigner, M. Gomina, Toward the enhancement of thermoelectric properties of lamellar $Ca_3Co_4O_9$ by edge-free spark plasma texturing, Scr. Mater. 66 (2012) 258–260.
[23] A. Sotelo, F.M. Costa, N.M. Ferreira, A. Kovalevsky, M.C. Ferro, V.S. Amaral, J.S. Amaral, Sh. Rasekh, M.A. Torres, M.A. Madre, J.C. Diez, Tailoring $Ca_3Co_4O_9$ microstructure and performances using a transient liquid phase sintering additive, J. Eur. Ceram. Soc. 36 (2016) 1025–1032.
[24] T. Schulz, J. Töpfer, Thermoelectric properties of $Ca_3Co_4O_9$ ceramics prepared by an alternative pressure-less sintering/annealing method, J. Alloys Compd. 659 (2016) 122–126.
[25] R. Kumar Gupta, R. Sharma, A.K. Mahapatro, R.P. Tandon, The effect of ZrO_2 dispersion on the thermoelectric power factor of $Ca_3Co_4O_9$, Phys. B 483 (2016) 48–53.
[26] K.T. Jacob, P. Gupta, Oxygen potentials and phase equilibria in the system Ca–Co–O and thermodynamic properties of $Ca_3Co_2O_6$ and $Ca_3Co_4O_{9.163}$, J. Solid State Chem. 221 (2015) 57–65.
[27] M. Shikano, R. Funahashi, Electrical and thermal properties of single-crystalline $(Ca_2CoO_3)_{0.7}CoO_2$ with a $Ca_3Co_4O_9$ structure, Appl. Phys. Lett. 82 (2003) 1851–1853.
[28] R.E. Sudhakar, J.G. Noudem, S. Hébert, C. Goupil, Fabrication and properties of four-leg oxide thermoelectric modules, J. Phys. D. 38 (2005) 3751–3755.
[29] J.G. Noudem, S. Lemonnier, M. Prevel, E.R. Reddy, E. Guilmeau, C. Goupil, Thermoelectric ceramics for generators, J. Eur. Ceram. Soc. 28 (2008) 41–48.
[30] R. Funahashi, S. Urata, Fabrication and application of an oxide thermoelectric system, Int. J. Appl. Ceram. Technol. 4 (2007) 297–307.
[31] H. Muguerra, D. Grebille, An original disorder-order transition related to electronic and magnetic properties in the thermoelectric misfit phase $Ca_3Co_4O_9$, Acta. Cryst. B 64 (2008) 676–683.